

1 **High-resolution IR spectroscopy and imaging**
2 **based on graphene micro-emitters**

3

4 Kenta Nakagawa,^{1,2,‡} Yui Shimura,^{1,‡} Yusuke Fukazawa,¹ Ryosuke Nishizaki,¹ Shinichiro Matano,¹
5 and Hideyuki Maki^{1,3,*}

6

7 ¹Department of Applied Physics and Physico-Informatics, Keio University, 3-14-1 Hiyoshi,
8 Kohoku-ku, Yokohama, Kanagawa 223-8522, Japan.

9 ²Kanagawa Institute of Industrial Science and Technology (KISTEC), 705-1 Shimoimaizumi, Ebina,
10 Kanagawa 243-0435, Japan.

11 ³Center for Spintronics Research Network, Keio University, 3-14-1 Hiyoshi, Kohoku-ku, Yokohama,
12 Kanagawa 223-8522, Japan.

13 [‡]These authors contributed equally to this work.

14 *E-mail: maki@appi.keio.ac.jp

15

16 **Summary paragraph**

17 IR spectroscopy such as Fourier transform infrared spectroscopy (FTIR) are widely used for the
18 investigation of structure and the quantitative determination of substances in the fields of chemistry,
19 physics, biology, medicine, and astronomy, because the energy of IR absorption corresponds to the
20 energy for each vibrational transition in functional groups within molecules.^{1,2,3} Microscopic
21 imaging of FTIR is used for various practical applications, as it enables visualization of the
22 composition distribution and changes in molecular structure without fluorescent labels.^{4,5,6,7}
23 However, FTIR microscopy with an objective lens has a diffraction limit causing the low spatial
24 resolution with the order of 10 μm .^{3,8,9} Here, we present high-spatial-resolution IR spectroscopy and
25 imaging based on graphene micro-emitters, which have distinct features over conventional IR
26 sources: a planar structure, bright intensity, a small footprint (sub μm^2), and high modulation speed
27 of ~ 100 kHz. We performed IR absorption spectroscopy on a polymer thin film using graphene
28 micro-emitters, realizing high-resolution IR imaging with a spatial resolution of ~ 2 μm , far higher
29 than that of the conventional FTIR. We show the two-dimensional IR chemical imaging that
30 visualizes the distribution of the chemical information, such as molecular species and functional
31 groups. This technique can open new routes for novel IR imaging and microanalysis in material

32 science, physics, chemistry, biology, and medicine.

33

34 **Main text**

35 The diffraction limit poses a challenge in developing higher-spatial-resolution FTIR.
36 FTIR spectroscopy with an attenuated total reflection crystal is a high-resolution imaging method,
37 which extends the diffraction limit by using a high refractive index crystal.^{1,2,3} Atomic force
38 microscope-IR (AFM-IR) spectroscopy^{10,11,12,13,14,15,16,17,18} and scattering scanning near-field optical
39 microscopy (s-SNOM)^{17,18,19,20,21,22,23,24,25,26,27,28} are methods that extend beyond the diffraction limit
40 of a scanning probe microscope. Although these probe-based methods can realize a high spatial
41 resolution of ~10 nm, an external coherent and strong IR source, such as a tunable IR laser, is
42 required as the strong beam should be focused on the probe tip. However, these tunable IR lasers
43 have very narrow wavelength range, and are also extremely expensive and large, compared with
44 incoherent thermal IR sources, such as incandescent light sources. Moreover, in probe-based IR
45 microscopy, the information for an IR absorption spectra needs to be indirectly extracted from
46 higher-order, modulated, or interferometric signals generated by tip vibration, pulsed laser, or
47 interferometer. The complicated interpretation of the measured signal required for their analyses is in
48 contrast to conventional FTIR.

49 In this study, we propose novel high-resolution IR absorption spectroscopy and imaging

50 using a graphene micro-emitter as an IR source. Graphene is promising as an IR light source owing
51 to its unique thermal properties, and enables a small footprint, high-speed, on-chip, and bright IR
52 emitter based on blackbody radiation by Joule heating can be fabricated.
53 ^{29,30,31,32,33,34,35,36,37,38,39,40,41,42,43,44} A graphene emitter does not require an external IR light source (a
54 tunable laser, etc.), so it can enable a small and simple IR spectroscopic technique by the direct
55 modulation of a graphene micro-emitter. In addition, the size of the graphene emitter can be
56 precisely controlled by a micro-fabrication technique in the sub-micrometer range, which is 10^{-6}
57 times smaller in area than conventional IR light sources such as incandescent light sources, because
58 graphene can be easily formed by dry-etching processes. Moreover, the graphene micro-emitter can
59 have direct contact with the measured sample, because it has a planar structure with an exposed
60 emitting layer. These features of graphene micro-emitters are advantageous for high-resolution IR
61 imaging. In this study, we fabricated small and bright graphene micro-emitters suitable for IR
62 analysis and successfully demonstrated its application in IR spectroscopy and high-resolution IR
63 imaging.

64 Blackbody emitters (exactly gray body emitters) with graphene as IR light sources were
65 fabricated on silicon chips. To ensure a small footprint and bright emission, we fabricated the emitter

66 using freely suspended graphene (Fig. 1a).³⁴ An emitter from unsuspended graphene was also used
67 as a mechanically stable emitter (Extended Data Fig. 1a).²⁹ For the emitter with suspended graphene,
68 a high temperature can be realized by Joule heating owing to low heat dissipation to a substrate, and
69 the bright blackbody emission can be obtained according to Stefan-Boltzmann law.³⁴ Details of the
70 fabrication methods of these emitters are described in Methods. Briefly, graphene was transferred on
71 a SiO₂ (1500 nm)/Si substrate using a mechanical exfoliation technique. Pd/Cr electrodes were
72 deposited on the graphene as source and drain electrodes. Suspended graphene was formed by SiO₂
73 etching using vapor HF. The size of the graphene channel was $5 \times 5 \mu\text{m}^2$ for suspended graphene
74 and $0.5 \times 0.5 \mu\text{m}^2$ or $10 \times 10 \mu\text{m}^2$ for unsuspended graphene. The fabricated chips were mounted on
75 chip carriers and were wire-bonded (Fig. 1a). A near-IR camera image of the thermal emission is
76 observed under a DC bias voltage ($V_{\text{ds}}=1.4$ V) in vacuum (Fig. 1b). Bright visible emission can also
77 be observed by a visible camera despite a low bias operation, indicating that the temperature of
78 graphene is remarkably high (Fig. 1b inset).

79 For application in IR analyses of spectroscopy and imaging, we investigated the emission
80 properties of this emitter in mid-IR region. Figure 1c shows the emission spectra (wavelength from
81 2.8 to 4.2 μm under a bias voltage from 1.25 to 1.4 V). Broad emission spectra can be obtained,

82 indicating the blackbody (gray body) radiation generated by Joule heating. The graphene
83 temperatures, obtained by the fitting of Planck's law,⁴⁵ are estimated to be 1238, 1340, 1455, and
84 1596 K at $V_{p-p}=1.25$ V, 1.3 V, 1.35 V, and 1.4 V, respectively. These temperatures are significantly
85 higher than the previously reported emitters with unsuspended graphene owing to the suppression of
86 heat dissipation to the substrate^{29,30,31,32,33,35,36,37,38,39,41,42,44} and are consistent with the previously
87 reported temperatures in the emitter with the suspended graphene.³⁴

88 Previous reports revealed that the emitter with unsuspended graphene has high
89 modulation speed (>1 GHz for single and few layer graphene and several tens MHz for multilayer
90 graphene).²⁹ We investigated the modulation speed of suspended graphene emitters. Figure 1d shows
91 that the frequency dependences of the light emission intensity were measured by a lock-in amplifier
92 and a spectrum analyzer. In this emitter with suspended graphene, the 3 dB bandwidth of the
93 emission intensity is ~125 kHz, which is slower than that of an unsuspended graphene emitter,
94 because the relaxation time of the graphene temperature is roughly inversely proportional to the heat
95 dissipation to the outside of graphene in the simple thermal model.^{29,46,47} However, the bandwidth of
96 125 kHz in our emitter is $\sim 10^4$ times faster than that in commercially available high-speed IR light
97 sources (~ 10 Hz) (see Methods and Extended Data Fig. 1c for details). This high-speed modulation

98 can be qualitatively understood by the small heat capacity of graphene owing to an atom-thick
99 substance. These results indicate that the small-footprint, bright, and high-speed blackbody emitters
100 with suspended graphene are suitable for microanalysis system in the IR region. The graphene
101 micro-emitter can realize high spatial resolution of IR spectroscopy and imaging. The high-speed
102 emitter enables the direct modulation of IR light without a light chopper, and this can contribute to
103 downsizing of the analysis system with a lock-in amplifier.

104 In this study, we propose a novel analysis system based on IR spectroscopy and imaging
105 using a graphene-based IR micro-emitter, as shown in Fig. 1e. In this system, the sample is placed
106 over the graphene micro-emitter and is irradiated by IR light. The local IR absorption transmitted
107 through the sample can be directly obtained. Figure 1f shows the schematic picture of the
108 constructed analysis system (see Methods for further details of set-up and measurements). The
109 graphene micro-emitter and the sample mounted to the three-axis stage are placed in the vacuum
110 chamber with an optical window, and the IR light which passes through the sample from the
111 graphene micro-emitter is corrected by an objective lens. The IR light is measured by two different
112 detectors: One is the isolated HgCdTe (MCT) detector, which can directly detect the IR light for
113 high-resolution imaging, and the other is the MCT detector with a monochromator, which can

114 measure the IR spectra for spectroscopy and wavelength-dependent imaging (i.e., chemical imaging).
115 The electrical signal from the MCT detector is measured by a lock-in amplifier, where the IR light
116 from the graphene emitter is directly modulated by applying a rectangular voltage input at 1113 Hz.
117 This is a great feature of the graphene emitter compared with the conventional IR sources, because
118 the high-speed direct modulation can be realized. This direct modulation can also contribute to
119 improved measurement sensitivity as the synchronized IR light to the graphene emission can be
120 selectively measured by a lock-in amplifier without the influence of environmental thermal
121 radiation.

122 We measured absorption spectra of spin-coated polymer thin films on quartz substrate by
123 using a suspended graphene micro-emitter ($5 \times 5 \mu\text{m}^2$). Figure 2a shows the absorption spectra of a
124 polymethyl methacrylate (PMMA) film measured by the graphene-based system and conventional
125 FTIR. Absorption peaks corresponding to the overtone of ester CH_3 deformation, CH_3 (ester methyl)
126 stretching mode, and CH_3 (α -methyl) stretching mode of PMMA⁴⁸ can be clearly observed at 2841
127 cm^{-1} , 2950 cm^{-1} , and 2994 cm^{-1} , respectively, which is consistent with the FTIR spectra. We also
128 measured the absorption spectra of polystyrene (PS), as shown in Fig. 2b, and absorption peaks
129 corresponding to CH_2 symmetric stretching mode, CH_2 asymmetric stretching mode, and aromatic

130 CH stretching mode of PS⁴⁸ can be observed at 2850 cm⁻¹, 2924 cm⁻¹, and 3000–3100 cm⁻¹,
131 respectively, corresponding to the FTIR spectra.

132 In general, the light intensity detected through a interferometer in FTIR is approximately
133 50% of the energy incident to the spectrometer, whereas the light intensity detected by a
134 monochromator reaches only a few percent of the energy incident to the spectrometer according to
135 so-called Jacquinot advantage.^{3,49} Moreover, the graphene microemitter has extremely small
136 footprint, which is approximately 10⁻⁶ times smaller in area than the ceramic IR sources for FTIR (~
137 mm²). Nevertheless, clear absorption peaks can be observed in the IR spectra measured by the
138 graphene micro-emitter coincide with those of a traditional FTIR. This indicates that graphene
139 micro-emitters are useful for IR spectroscopy, and it is possible to analyze the local molecular
140 structures of substances.

141 We also demonstrated high-resolution IR imaging using an unsuspended graphene
142 micro-emitter with the sub-micrometer size of 0.5 × 0.5 μm² (the details are described in Methods).
143 Since the specimen is mounted to the three-axis stage, the specimen can be precisely approached to
144 the graphene emitter, and an infrared absorption image can be obtained by scanning the specimen in
145 the *XY* plane.

146 To evaluate the spatial resolution of the infrared absorption imaging, we measured
147 linearly scanned IR absorption of the Ni line and space pattern with the linewidth of 20, 10, 5, and 2
148 μm fabricated by lithography technique on quartz substrate, as shown in Fig. 3a. Figure 3b shows
149 the one-dimensional transmittance along X and Y axes. The periodical contrast of transmittance,
150 which is owing to the masking of IR light by the Ni line, can be clearly observed for the linewidth of
151 $\geq 2 \mu\text{m}$, a spatial resolution sufficiently higher than conventional FTIR microscopy (see Extended
152 Data Fig. 3).

153 With IR imaging using a graphene micro-emitter, it is expected that the spatial resolution
154 of the imaging is determined by the size of the graphene micro-emitter. To elucidate this, we
155 measured the spatial resolution of this system with shifting the focus of the objective lens. Here, the
156 one-dimensional line scan was performed while shifting the focus of the objective lens in the $\pm z$
157 direction ($|\Delta z|=50 \mu\text{m}$), as shown in Fig. 3c. Surprisingly, no line-profile change is observed with
158 changing the position of the objective lens, indicating that spatial resolution is not dependent on the
159 focus of the objective lens, as shown in Fig. 3d. Here, as the numerical aperture NA of the objective
160 lens used in this study is 0.5, the spot-size diameter D of the defocused objective is given by
161 $D=2|\Delta z|\tan(\sin^{-1}\text{NA})\approx 57.7 \mu\text{m}$, which is significantly larger than the width of the line and space.

162 Nevertheless, the clear profile of the line scan with the spatial resolution of $\sim 2 \mu\text{m}$ can be obtained,
163 independent of the objective focusing. This indicates that spatial resolution can be determined by the
164 size of graphene micro-emitter. The contribution of this size effect to the spatial resolution is
165 maximized on minimizing the gap between the graphene micro-emitter and the sample. As the
166 graphene micro-emitter can be in direct contact with the measured sample, high spatial resolution of
167 IR imaging can be realized by using graphene micro-emitters.

168 To demonstrate high-resolution two-dimensional infrared absorption imaging with a
169 graphene micro-emitter, we measured a $5 \mu\text{m}$ width '5'-shaped Ni pattern fabricated by
170 photolithography on a quartz substrate as shown in the optical microscope image of Fig. 3e. This
171 patterned specimen was contacted to the graphene micro-emitter and was scanned in the *XY* plane.
172 The two-dimensional image of the transmittance is shown in Fig. 3f. An IR image corresponding to
173 the '5'-shaped pattern can be clearly observed. Notably, the spatial resolution of this IR image by the
174 graphene micro-emitter is significantly higher than by conventional FTIR microscope, as shown in
175 Fig. 3g, in which the image is blurred and the '5' shape cannot be clearly identified.

176 We also demonstrated IR chemical imaging that visualizes the two-dimensional
177 distribution of chemical information, such as molecular species and functional groups using an

178 unsuspended graphene micro-emitter with the size of $10 \times 10 \mu\text{m}^2$. Here, we measured the
179 position-dependent IR absorption spectra and two-dimensional IR absorption imaging at the specific
180 wavelength using a monochromator. In this study, the photoresist polymer (ZPN1150) showed broad
181 absorption peaks corresponding to the O-H and C-H stretching modes at $3.0 \mu\text{m}$ (3333 cm^{-1}) and 3.4
182 μm (2941 cm^{-1}), respectively (Fig. 4a). A $50 \mu\text{m}$ width '6'-shaped polymer pattern was fabricated by
183 photolithography on a quartz substrate (Fig. 4b). The IR chemical image of this polymer pattern was
184 measured by scanning the specimen in the *XY* plane and measuring the position-dependent
185 absorption spectra. Figure 4c shows the line scan result of absorption spectra along the black broken
186 line on the polymer pattern in Fig. 4b. Clear absorption can be observed at 3.0 and $3.4 \mu\text{m}$ owing to
187 O-H and C-H stretching modes on the polymer, respectively. Figure 4d, 4e, and 4f shows
188 two-dimensional absorption imaging at the wavelength of $2.5 \mu\text{m}$ (no absorption), $3.0 \mu\text{m}$ (O-H
189 absorption), and $3.4 \mu\text{m}$ (C-H absorption), respectively. No image can be observed at $2.5 \mu\text{m}$ (Fig.
190 4d), because there is no absorption at this wavelength as shown in Fig. 4a and 4c. Notably, the slight
191 decrease of the transmittance can be observed at the edge of the polymer pattern due to the light
192 scattering at the edge of the pattern. On the other hand, absorption images, consistent with the
193 polymer pattern in Fig. 4b, can be clearly observed at 3.0 and $3.4 \mu\text{m}$, corresponding to O-H and

194 C-H stretching modes, as shown in Fig. 4e and 4f, respectively. These results indicate that the
195 two-dimensional IR chemical images can be obtained by scanning the graphene micro-emitter, and
196 this IR analysis based on the graphene micro-emitter is a novel spatial and spectral analysis.

197 In conclusion, we have developed and demonstrated high-resolution IR spectroscopy and
198 imaging using graphene micro-emitters. The graphene micro-emitter has the advantages of bright
199 intensity, smaller footprint and diffraction limit, and high modulation speed on silicon chips for this
200 novel IR analysis, in contrast to conventional IR sources. This distinct graphene micro-emitter can
201 realize local IR analysis, whose spatial resolution is determined by the size of the graphene
202 micro-emitter. In addition, the high-resolution IR imaging, including the spatial distribution of the
203 chemical information, such as molecular species and functional groups, can also be obtained by
204 scanning the graphene emitter. As the expected size of the graphene light emitters can be ~10 nm in
205 the future,⁵⁰ this analysis method has potential in higher-resolution IR microscopy, which is
206 comparable to probe-based IR microscopy, such as AFM-IR and s-SNOM. Furthermore, this method
207 has distinct advantages from AFM-IR and s-SNOM that this graphene-based IR analysis system can
208 be inexpensively and simply constructed because (i) the external tunable laser, which is ultrabright,
209 large, and expensive, is not required, (ii) the wide wavelength range can be easily measured by using

210 the graphene blackbody emitter compared with the tunable laser, and (iii) the IR spectra can be
211 directly obtained by the simple optical set-up and signal processing, in contrast with the complicated
212 interpretation obtained from the higher-order, modulated, or interferometric signal in AFM-IR and
213 s-SNOM. Hence, this IR spectroscopy and microscopy based on graphene micro-emitters can open
214 the door to nanoscale analytical chemistry by the structure and quantitative analysis for any
215 ultra-small matter, such as nanomaterials, biological samples, difficult synthesis substances, and
216 hazardous substances.

217

218 **References**

- 219 1. Günter Gauglitz and David S. Moore. *Handbook of Spectroscopy: Second, Enlarged Edition*.
220 (WILEY-VCH, 2014).
- 221 2. Salzer, R. & Siesler, H. W. *Infrared and Raman Spectroscopic Imaging*. (WILEY-VCH, 2009).
- 222 3. Griffiths, P. R. & de Haseth, J. A. *Fourier Transform Infrared Spectrometry (Second Edition)*.
223 (Wiley-Interscience, 2007).
- 224 4. Levin, I. W. & Bhargava, R. Fourier Transform Infrared Vibrational Spectroscopic Imaging:
225 Integrating Microscopy and Molecular Recognition. *Annu. Rev. Phys. Chem.* **56**, 429–474 (2005).
- 226 5. Sergei G. Kazarian & Chan, K. L. A. Micro- and Macro- Attenuated Total Reflection Fourier
227 Transform Infrared Spectroscopic Imaging. *Appl. Spectrosc.* **64**, 135A-152A (2010).
- 228 6. Bhargava, R. Infrared spectroscopic imaging: The next generation. *Appl. Spectrosc.* **66**, 1091–
229 1120 (2012).
- 230 7. Bellisola, G. & Sorio, C. Infrared spectroscopy and microscopy in cancer research and diagnosis.
231 *Am. J. Cancer Res.* **2**, 1–21 (2012).
- 232 8. Abbe, E. Beiträge zur Theorie des Mikroskops und der mikroskopischen Wahrnehmung. *Arch.*
233 *für Mikroskopische Anat.* **9**, 413–468 (1873).

- 234 9. McCutchen, C. W. Superresolution in microscopy and the Abbe resolution limit. *J. Opt. Soc. Am.*
235 **57**, 1190–1192 (1967).
- 236 10. Dazzi, A., Prazeres, R., Glotin, F. & Ortega, J. M. Local infrared microspectroscopy with
237 subwavelength spatial resolution with an atomic force microscope tip used as a photothermal
238 sensor. *Opt. Lett.* **30**, 2388–2390 (2005).
- 239 11. Dazzi, A., Glotin, F. & Carminati, R. Theory of infrared nanospectroscopy by photothermal
240 induced resonance. *J. Appl. Phys.* **107**, 124519 (2010).
- 241 12. Lu, F. & Belkin, M. A. Infrared absorption nano-spectroscopy using sample photoexpansion
242 induced by tunable quantum cascade lasers. *Opt. Express* **19**, 19942–19947 (2011).
- 243 13. Lu, F., Jin, M. & Belkin, M. A. Tip-enhanced infrared nanospectroscopy via molecular expansion
244 force detection. *Nat. Photonics* **8**, 307–312 (2014).
- 245 14. Ramer, G., Reisenbauer, F., Steindl, B., Tomischko, W. & Lendl, B. Implementation of
246 Resonance Tracking for Assuring Reliability in Resonance Enhanced Photothermal Infrared
247 Spectroscopy and Imaging. *Appl. Spectrosc.* **71**, 2013–2020 (2017).
- 248 15. Dazzi, A. *et al.* AFM–IR: Combining Atomic Force Microscopy and Infrared Spectroscopy for
249 Nanoscale Chemical Characterization. *Appl. Spectrosc.* **66**, 1365–1384 (2012).

- 250 16. Dazzi, A. & Prater, C. B. AFM-IR: Technology and applications in nanoscale infrared
251 spectroscopy and chemical imaging. *Chem. Rev.* **117**, 5146–5173 (2017).
- 252 17. Centrone, A. Infrared Imaging and Spectroscopy Beyond the Diffraction Limit. *Annu. Rev. Anal.*
253 *Chem.* **8**, 101–126 (2015).
- 254 18. Xiao, L. & Schultz, Z. D. Spectroscopic Imaging at the Nanoscale: Technologies and Recent
255 Applications. *Anal. Chem.* **90**, 440–458 (2018).
- 256 19. Keilmann, F. & Hillenbrand, R. Near-field microscopy by elastic light scattering from a tip.
257 *Philos. Trans. R. Soc. A Math. Phys. Eng. Sci.* **362**, 787–805 (2004).
- 258 20. Huth, F., Schnell, M., Wittborn, J., Ocelic, N. & Hillenbrand, R. Infrared-spectroscopic
259 nanoimaging with a thermal source. *Nat. Mater.* **10**, 352–356 (2011).
- 260 21. Huth, F. *et al.* Nano-FTIR absorption spectroscopy of molecular fingerprints at 20 nm spatial
261 resolution. *Nano Lett.* **12**, 3973–3978 (2012).
- 262 22. Govyadinov, A. A., Amenabar, I., Huth, F., Scott Carney, P. & Hillenbrand, R. Quantitative
263 measurement of local infrared absorption and dielectric function with tip-enhanced near-field
264 microscopy. *J. Phys. Chem. Lett.* **4**, 1526–1531 (2013).
- 265 23. Amenabar, I. *et al.* Structural analysis and mapping of individual protein complexes by infrared

- 266 nanospectroscopy. *Nat. Commun.* **4**, 2890 (2013).
- 267 24. Berweger, S. *et al.* Nano-chemical infrared imaging of membrane proteins in lipid bilayers. *J. Am.*
268 *Chem. Soc.* **135**, 18292–18295 (2013).
- 269 25. Mastel, S., Govyadinov, A. A., de Oliveira, T. V. A. G., Amenabar, I. & Hillenbrand, R.
270 Nanoscale-resolved chemical identification of thin organic films using infrared near-field
271 spectroscopy and standard Fourier transform infrared references. *Appl. Phys. Lett.* **106**, 023113
272 (2015).
- 273 26. Muller, E. A., Pollard, B. & Raschke, M. B. Infrared chemical nano-imaging: Accessing structure,
274 coupling, and dynamics on molecular length scales. *J. Phys. Chem. Lett.* **6**, 1275–1284 (2015).
- 275 27. Tranca, D. E. *et al.* High-resolution quantitative determination of dielectric function by using
276 scattering scanning near-field optical microscopy. *Sci. Rep.* **5**, 11876 (2015).
- 277 28. Amenabar, I. *et al.* Hyperspectral infrared nanoimaging of organic samples based on Fourier
278 transform infrared nanospectroscopy. *Nat. Commun.* **8**, 14402 (2017).
- 279 29. Miyoshi, Y. *et al.* High-speed and on-chip graphene blackbody emitters for optical
280 communications by remote heat transfer. *Nat. Commun.* **9**, 1279 (2018).
- 281 30. Freitag, M., Chiu, H. Y., Steiner, M., Perebeinos, V. & Avouris, P. Thermal infrared emission

- 282 from biased graphene. *Nat. Nanotechnol.* **5**, 497–501 (2010).
- 283 31. Luxmoore, I. J. *et al.* Thermal emission from large area chemical vapor deposited graphene
284 devices. *Appl. Phys. Lett.* **103**, 131906 (2013).
- 285 32. Lawton, L. M., Mahlmeister, N. H., Luxmoore, I. J. & Nash, G. R. Prospective for graphene
286 based thermal mid-infrared light emitting devices. *AIP Adv.* **4**, 087139 (2014).
- 287 33. Nakagawa, K., Takahashi, H., Shimura, Y. & Maki, H. A light emitter based on practicable and
288 mass-producible polycrystalline graphene patterned directly on silicon substrates from a
289 solid-state carbon source. *RSC Adv.* **9**, 37906–37910 (2019).
- 290 34. Kim, Y. D. *et al.* Bright visible light emission from graphene. *Nat. Nanotechnol.* **10**, 676–681
291 (2015).
- 292 35. Kim, Y. D. *et al.* Ultrafast Graphene Light Emitters. *Nano Lett.* **18**, 934–940 (2018).
- 293 36. Barnard, H. R. *et al.* Boron nitride encapsulated graphene infrared emitters. *Appl. Phys. Lett.* **108**,
294 131110 (2016).
- 295 37. Berciaud, S. *et al.* Electron and optical phonon temperatures in electrically biased graphene. *Phys.*
296 *Rev. Lett.* **104**, 227401 (2010).
- 297 38. Bae, M. H., Ong, Z. Y., Estrada, D. & Pop, E. Imaging, simulation, and electrostatic control of

- 298 power dissipation in graphene devices. *Nano Lett.* **10**, 4787–4793 (2010).
- 299 39. Bae, M. H., Islam, S., Dorgan, V. E. & Pop, E. Scaling of high-field transport and localized
300 heating in graphene transistors. *ACS Nano* **5**, 7936–7944 (2011).
- 301 40. Grosse, K. L., Bae, M. H., Lian, F., Pop, E. & King, W. P. Nanoscale Joule heating, Peltier
302 cooling and current crowding at graphene-metal contacts. *Nat. Nanotechnol.* **6**, 287–290 (2011).
- 303 41. Mahlmeister, N. H., Lawton, L. M., Luxmoore, I. J. & Nash, G. R. Modulation characteristics of
304 graphene-based thermal emitters. *Appl. Phys. Express* **9**, 012105 (2016).
- 305 42. Engel, M. *et al.* Light-matter interaction in a microcavity-controlled graphene transistor. *Nat.*
306 *Commun.* **3**, 906 (2012).
- 307 43. Shi, C., Mahlmeister, N. H., Luxmoore, I. J. & Nash, G. R. Metamaterial-based graphene thermal
308 emitter. *Nano Res.* **11**, 3567–3573 (2018).
- 309 44. Luo, F. *et al.* Graphene Thermal Emitter with Enhanced Joule Heating and Localized Light
310 Emission in Air. *ACS Photonics* **6**, 2117–2125 (2019).
- 311 45. Planck, M. On the Law of the Energy Distribution in the Normal Spectrum. *Ann. Phys.* **4**, 553–
312 564 (1901).
- 313 46. Vora, H., Kumaravadivel, P., Nielsen, B. & Du, X. Bolometric response in graphene based

- 314 superconducting tunnel junctions. *Appl. Phys. Lett.* **100**, 153507 (2012).
- 315 47. Yan, J. *et al.* Dual-gated bilayer graphene hot-electron bolometer. *Nat. Nanotechnol.* **7**, 472–478
316 (2012).
- 317 48. Mark, J. E. *Physical Properties of Polymers Handbook Second Edition.* Springer (2007).
318 doi:10.1007/978-0-387-69002-5_3.
- 319 49. Griffiths, P. R., Sloane, H. J. & Hannah, R. W. Interferometers vs Monochromators: Separating
320 the Optical and Digital Advantages. *Appl. Spectrosc.* **31**, 485–495 (1977).
- 321 50. Xu, W. & Lee, T. W. Recent progress in fabrication techniques of graphene nanoribbons. *Mater.*
322 *Horizons* **3**, 186–207 (2016).
- 323 51. Pop, E., Varshney, V. & Roy, A. K. Thermal properties of graphene: Fundamentals and
324 applications. *MRS Bull.* **37**, 1273–1281 (2012).

325

326

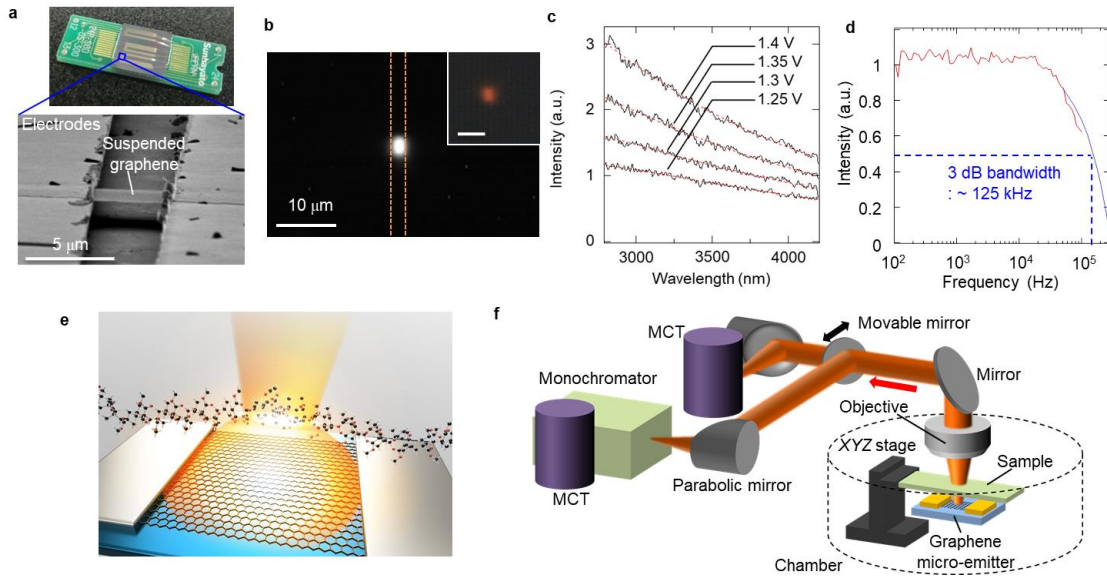
327 **Acknowledgments**

328 We thank Ms. S. Sugimoto and Mr. R. Mogi of Keio University, Dr. K. Iwami of Tokyo
329 University of Agriculture and Technology for their technical supports. This work was partially
330 financially supported by Kanagawa Institute of Industrial Science and Technology (KISTEC),
331 PRESTO (Grant Number JPMJPR152B) from JST and KAKENHI (Grant Number 16H04355,
332 23686055, 18K19025, and 20H02210). This work was technically supported by Spintronics
333 Research Network of Japan, the Core-to-Core program from JSPS, and NIMS Nanofabrication
334 Platform in Nanotechnology Platform Project by MEXT.

335

336

337 **Figures**



338

339 **Fig.1 | Graphene micro-emitters and IR analysis system. a,** A fabricated micro-emitter with

340 suspended graphene on a silicon chip, which is mounted on a chip carrier. **b,** IR and visible (inset)

341 camera images of the light emission from the suspended graphene micro-emitter ($5 \times 5 \mu\text{m}^2$) at

342 $V_{ds}=1.4$ V. **c,** Emission spectra from the suspended graphene micro-emitter ($5 \times 5 \mu\text{m}^2$) for

343 $V_{p-p}=1.25\text{--}1.4$ V with a step of 0.05 V. The red curves are fitted according to Planck's law. **d,**

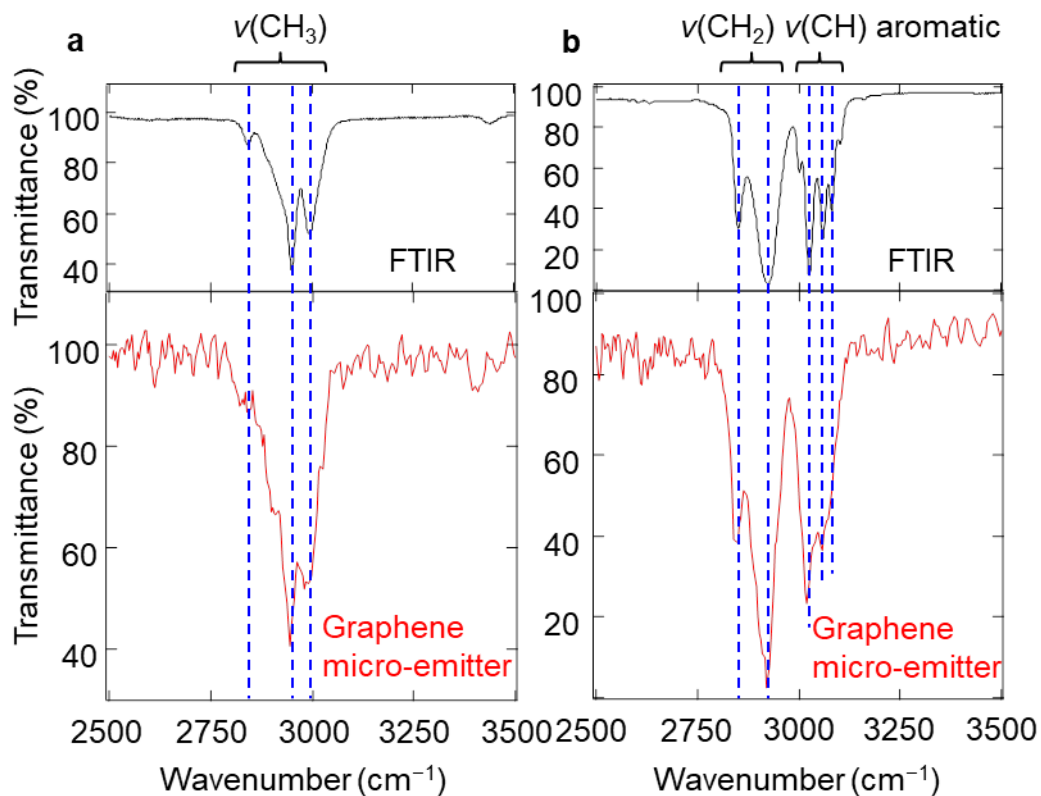
344 Frequency dependence of the light emission intensity of the suspended graphene micro-emitter ($5 \times$

345 $5 \mu\text{m}^2$). The red and blue curves show the data obtained by a lock-in amplifier and a spectrum

346 analyzer, respectively. **e,** Schematic of the graphene micro-emitter-based IR analysis. IR light from

347 graphene micro-emitter is irradiated to the specimen, and the transmitted light through the specimen

348 is measured for IR absorption spectroscopy and imaging. **f**, Schematic of the IR analysis system. IR
349 light generated from graphene micro-emitter is irradiated to the sample, which can be manipulated
350 on a *XYZ* stage. The transmitted light through a specimen is corrected by an objective lens and is
351 guided to the isolated MCT detector or the monochromator with an MCT detector for
352 high-resolution imaging or spectroscopy, respectively
353



354

355 **Fig.2 | IR absorption spectra. a,b**, IR absorption spectra of the polymethyl methacrylate (a) and

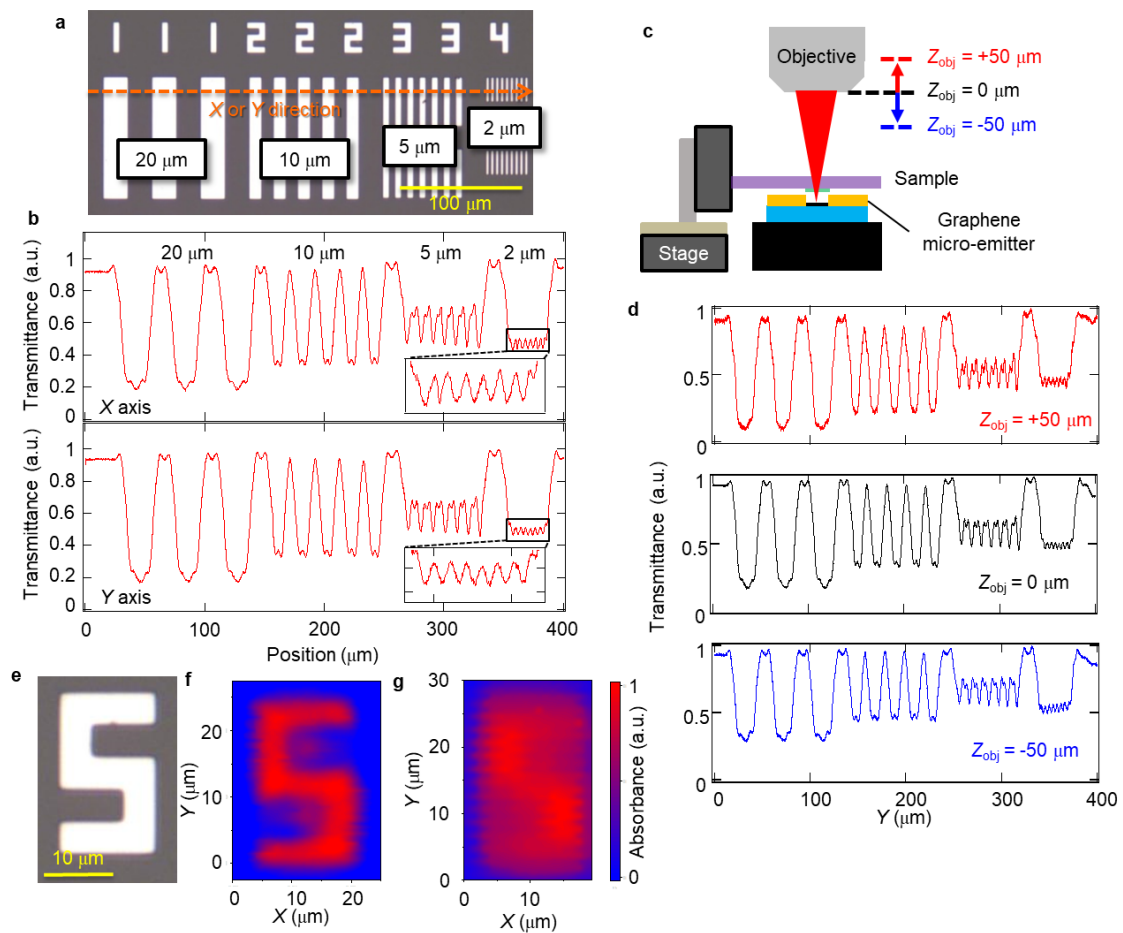
356 polystyrene (b). The upper and lower spectra are the IR absorption spectra measured by

357 conventional FTIR and the IR analysis system by using the suspended graphene micro-emitter (5×5

358 μm^2), respectively. The peak positions in the graphene-based IR spectra are coincident to that in the

359 conventional FTIR spectra

360



361

362 **Fig.3 | High-resolution IR absorption imaging. a,** Optical microscope image of the Ni line and

363 space pattern with the linewidth of 20, 10, 5, and 2 μm. The specimen was moved along the orange

364 arrow, and the transmitted light intensity at each position was measured (one-dimensional line scan).

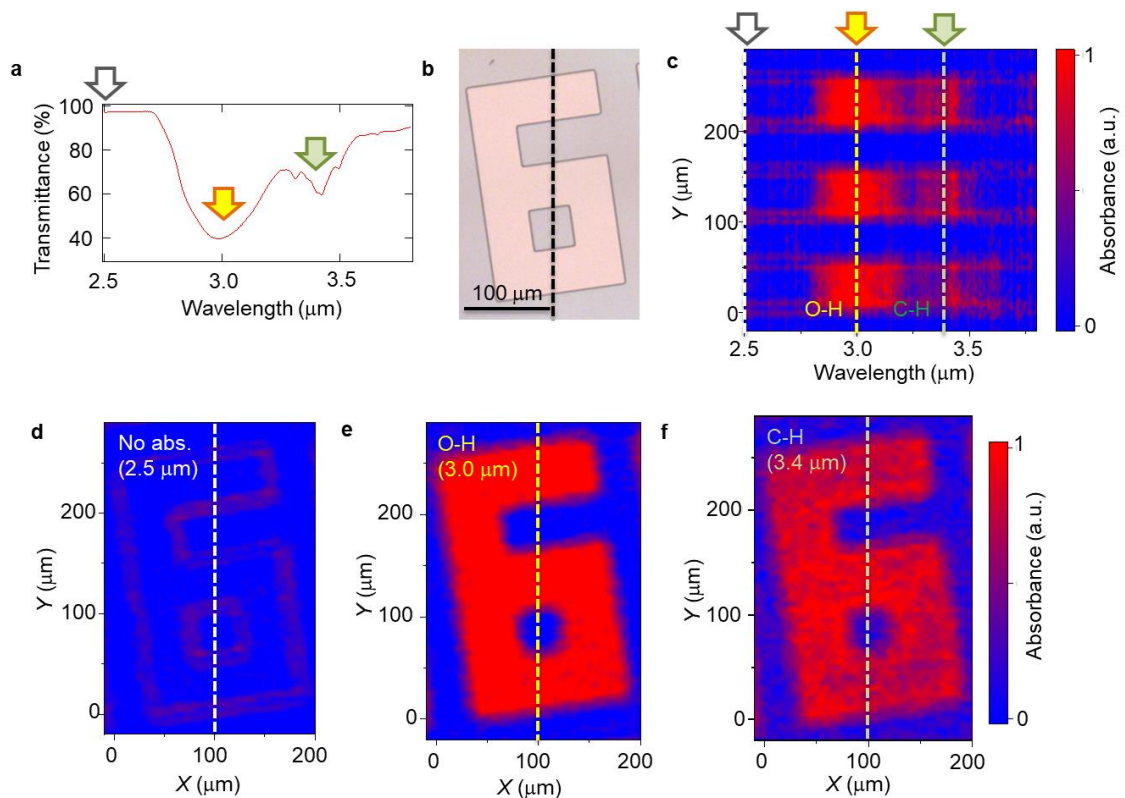
365 **b,** Transmittance of one-dimensional line scan along the X and Y axes directions by using the

366 unsuspended graphene micro-emitter ($0.5 \times 0.5 \mu\text{m}^2$). The one-dimensional line scan was performed

367 by scanning the sample along X(Y) axis with a step of 100 nm. Clear periodical modulation of the

368 transmittance can be observed for all line/space pattern, indicating that spectral resolution is $\sim 2 \mu\text{m}$.

369 **c**, Schematic of the method of the objective position dependence of the spatial resolution.
370 One-dimensional line scan by using the unsuspended graphene micro-emitter ($0.5 \times 0.5 \mu\text{m}^2$) was
371 performed while shifting the focus of the objective lens in the $\pm z$ direction ($|\Delta z| = 50 \mu\text{m}$). **d**,
372 Objective position dependence of the spatial resolution. No line-profile change is observed with
373 changing the position of the objective lens, indicating that spatial resolution does not depend on
374 focusing of the objective lens. **e**, Optical microscope image of the '5'-shaped Ni pattern with the
375 linewidth of $5 \mu\text{m}$. **f**, **g**, Two-dimensional IR absorption imaging of the '5'-shaped Ni pattern in **e**
376 obtained by the unsuspended graphene micro-emitter ($0.5 \times 0.5 \mu\text{m}^2$) (**f**) and the conventional FTIR
377 (**g**). The two-dimensional IR absorption imaging by the graphene micro-emitter was performed by
378 scanning the sample in XY plane with a step of 500 nm . The spatial resolution of this IR image by
379 the graphene micro-emitter is significantly higher than that by the conventional FTIR microscope
380



381

382 **Fig. 4 | IR chemical imaging.** **a**, IR absorption spectrum for photoresist polymer (ZPN1150). Clear

383 dips are observed at 3.0 and 3.4 μm corresponding to the O-H and C-H stretching modes. White,

384 yellow, and green arrows indicate the wavelength of 2.5 μm (no absorption), 3.0 μm (O-H

385 absorption), and 3.4 μm (C-H absorption), respectively. **b**, Optical microscope image of the

386 '6'-shaped ZPN1150 pattern with the linewidth of 50 μm . **c**, Line scan result of absorption spectra

387 along the black broken line on the polymer pattern in **b** by using the unsuspended graphene

388 micro-emitter ($10 \times 10 \mu\text{m}^2$). White, yellow, and green arrows and broken lines correspond to the

389 arrows in **a**. The absorption spectra line scan was performed by scanning the sample along Y axis

390 with a step of 5 μm . **d, e, f**, Two-dimensional absorption imaging at the wavelength of 2.5 μm (no
391 absorption) (**d**), 3.0 μm (O-H absorption), (**e**) and 3.4 μm (C-H absorption) (**f**), respectively by using
392 the unsuspended graphene micro-emitter ($10 \times 10 \mu\text{m}^2$). The two-dimensional absorption imaging
393 was performed by scanning the sample in *XY* plane with a step of 5 μm
394

395 **Methods**

396 **Graphene micro-emitter fabrication**

397 Graphene is promising as an IR light source^{29,30,31,32,33,34,35,36,37,38,39,40,41,42,43,44} owing to its
398 unique two-dimensional thermal properties.⁵¹ In this study, single side polished Si wafers were used
399 as substrates. SiO₂ with a thickness of 1500 nm was deposited on the substrates by chemical vapor
400 deposition. Graphene is mechanically exfoliated from highly ordered pyrolytic graphite and
401 transferred onto the substrates. The graphene on the substrate was patterned by photolithography or
402 electron-beam lithography and O₂ plasma etching with a Ni mask, which was subsequently removed
403 by immersion in a HCl solution. Pd (145 nm)/Cr (5 nm) electrodes were deposited on the patterned
404 graphene by vacuum vapor deposition as source and drain electrodes. The sizes of the graphene
405 channels in this work were $5 \times 5 \mu\text{m}^2$ for the measurements in Figs. 1 and 2 (Extended Data Fig. 1b),
406 $0.5 \times 0.5 \mu\text{m}^2$ for the high-resolution imaging in Fig. 3 (Extended Data Fig. 3), and $10 \times 10 \mu\text{m}^2$ for
407 the chemical imaging in Fig. 4 (Extended Data Fig. 1a). For the experiments in Figs. 1 and 2
408 (Extended Data Fig. 1b), the graphene was suspended by SiO₂ etching using vapor HF (Fig. 1a). The
409 electrodes were wire-bonded by Al wires to connect electrically to a chip carrier (Fig. 1a). The
410 electronic property of the fabricated micro-emitters with the suspended graphene of $5 \times 5 \mu\text{m}^2$ shows

411 Ohmic conduction behavior, as shown in Extended Data Fig. 1b. Extended Data Fig. 1c shows the
412 frequency dependence of the emission intensity of the graphene micro-emitter with the unsuspended
413 graphene of $5 \times 5 \mu\text{m}^2$, in comparison with the conventional high-speed IR emitter (Hawkeye
414 Technologies). The graphene micro-emitter exhibits a stable frequency response over 10 kHz, which
415 is at least 1000 times faster than the conventional IR emitter.

416

417 **Optical measurements**

418 Optical measurements were carried out at room temperature in a high-vacuum chamber
419 (Fig. 1 and Extended Data Fig. 2). In the optical measurement, the emitted light from the graphene
420 micro-emitter was collected by an objective lens through the optical window of the vacuum chamber.
421 The emission image of the graphene micro-emitter under DC bias voltage (Fig. 1b) was directly
422 observed with an InGaAs CCD camera, which has the detection wavelength range from 900 to 1600
423 nm. For the detection of IR light by an MCT detector (detection range, 1–15 μm), which is used in
424 the measurement of emission spectra (Fig. 1c), absorption spectra (Fig. 2), IR imaging (Fig. 3), and a
425 chemical imaging (Fig. 4), graphene emission is modulated by applying a rectangular bias voltage of
426 1113 Hz (1:1 duty ratio) to the graphene micro-emitter by a function generator. In the IR analysis,

427 the specimen formed on the quartz substrate is mounted to the *XYZ* stage in the vacuum chamber,
428 and the IR light from the graphene micro-emitter is transmitted through the specimen under scanning
429 the sample (Fig. 1f and Extended Data Fig. 2). The transmitted IR light through the specimen is
430 corrected by a Cassegrain objective lens ($\times 40$) placed above the vacuum chamber through the
431 sapphire optical window. The collimated light from the objective lens is focused by a parabolic
432 mirror and is guided to an MCT detector directly or through a monochromator with a grating. The
433 intensity of IR light incident to the MCT detector is detected by a lock-in amplifier. The relative
434 spectral response of the optical system such as the optical path and the detector was measured with a
435 standard light from a blackbody furnace, and all spectra were corrected accordingly. For comparison
436 with this novel graphene-based IR analysis system, we measured IR absorption spectra and imaging
437 with the conventional FTIR [ALPHA (Bruker) for the spectra measurements and IRAffinity-1S and
438 AIM-9000 (Shimadzu) for the imaging measurements].

439 For the demonstration of the high-resolution IR imaging, we fabricated a sample with the
440 fine pattern of Ni lines and space pattern with the linewidth from 2 to 20 μm (Fig. 3a) and the 5 μm
441 linewidth '5'-shaped Ni pattern (Fig. 3e) on quartz substrates by photolithography technique. These
442 samples were mounted onto a *XYZ* piezo motor stage in the vacuum chamber. The sample was

443 brought into close contact with the graphene micro-emitters, and IR transmittance (absorption) were
444 obtained by scanning the sample along $X(Y)$ axis with a step of 100 nm for one-dimensional line
445 scan and in XY plane with a step of 500 nm for two-dimensional IR absorption imaging. Since a
446 mechanically stable and small-footprint graphene micro-emitter is necessary for the high resolution
447 imaging, we used an unsuspended graphene emitter with the sub-micrometer size of $0.5 \times 0.5 \mu\text{m}^2$.
448 As described in the main text and Fig. 3, the graphene-based IR analysis method has high spatial
449 resolution of $\sim 2 \mu\text{m}$. As shown in the line scan results of the conventional FTIR in Extended Data
450 Fig. 3, the spatial resolution of this method is significantly higher than that of the conventional FTIR
451 microscopy.

452 For the demonstration of the IR chemical imaging, we fabricated the 50- μm width
453 ‘6’-shaped polymer pattern of ZPN1150 photoresist (Zeon Corporation) on a quartz substrate (Fig.
454 4b). This polymer has absorption peaks of O-H and C-H stretching modes at 3.0 and 3.4 μm ,
455 respectively (Fig. 4a). Since a mechanically stable and bright graphene micro-emitter is necessary
456 for the simultaneous measurement of spectroscopy and imaging through a monochromator, we used
457 an unsuspended graphene micro-emitter with the large footprint of $10 \times 10 \mu\text{m}^2$ (Extended Data Fig.
458 1a). We measured the line scan of absorption spectra across the ‘6’-shaped polymer pattern along Y

459 axis with a step of 5 μm , where the absorption spectra are measured at each position. We also
460 measured the two-dimensional absorption imaging at the wavelength of 2.5 μm (no absorption), 3.0
461 μm (O-H absorption), and 3.4 μm (C-H absorption). In this imaging, the measured wavelength of the
462 grating in a monochromator is set to their wavelength, and the IR intensity through the sample is
463 measured under scanning in *XY* plane with the step of 5 μm .
464

465

Extended Data

466 **High-resolution IR spectroscopy and imaging** 467 **based on graphene micro-emitters**

468

469 Kenta Nakagawa,^{1,2,‡} Yui Shimura,^{1,‡} Yusuke Fukazawa,¹ Ryosuke Nishizaki,¹ Shinichiro Matano,¹
470 and Hideyuki Maki^{1,3,*}

471

472 ¹Department of Applied Physics and Physico-Informatics, Keio University, 3-14-1 Hiyoshi,
473 Kohoku-ku, Yokohama, Kanagawa 223-8522, Japan.

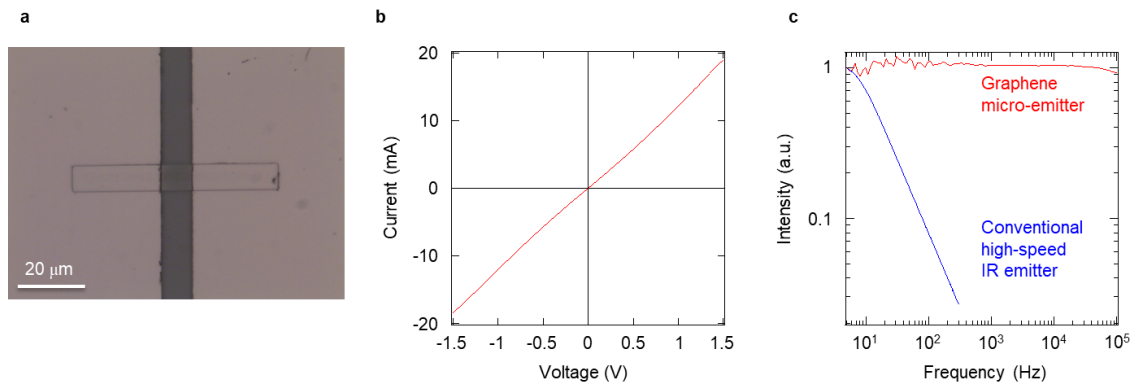
474 ²Kanagawa Institute of Industrial Science and Technology (KISTEC), 705-1 Shimoimaizumi, Ebina,
475 Kanagawa 243-0435, Japan.

476 ³Center for Spintronics Research Network, Keio University, 3-14-1 Hiyoshi, Kohoku-ku, Yokohama,
477 Kanagawa 223-8522, Japan.

478 [‡]These authors contributed equally to this work.

479 *E-mail: maki@appi.keio.ac.jp

480



481

482 **Extended Data Fig. 1 | Graphene micro-emitter.** **a**, Optical microscope image of the unsuspended

483 graphene micro-emitter with the size of $10 \times 10 \mu\text{m}^2$. **b**, DC bias voltage (V_{ds}) dependence of the

484 current I (I - V_{ds} curve) of the suspended graphene micro-emitter with the size of $5 \times 5 \mu\text{m}^2$. The

485 fabricated micro-emitters show Ohmic conduction behavior. **c**, Frequency dependence of the

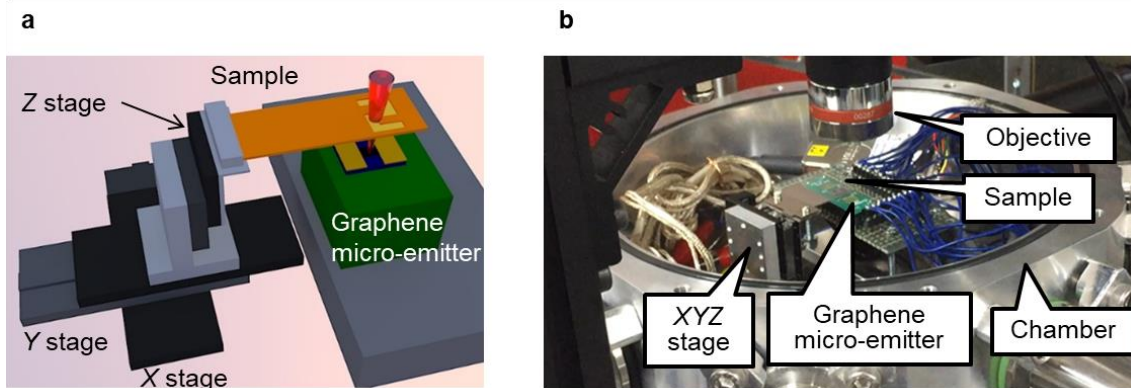
486 emission intensity of the unsuspended graphene micro-emitter with the size of $5 \times 5 \mu\text{m}^2$, in

487 comparison with the conventional high-speed IR emitter (Hawkeye Technologies). The graphene

488 micro-emitter exhibits stable frequency response over 10 kHz, which is at least 1000 times faster

489 than the conventional IR emitter

490



491

492 **Extended Data Fig. 2 | System in the IR system vacuum chamber. a,b**, Schematic image (a) and

493 photograph (b) of the system in the IR analysis system vacuum chamber. In the analysis vacuum

494 chamber, the specimen is mounted to the XYZ stage, and the IR light from the graphene

495 micro-emitter is transmitted through the sample. The transmitted IR light through the specimen is

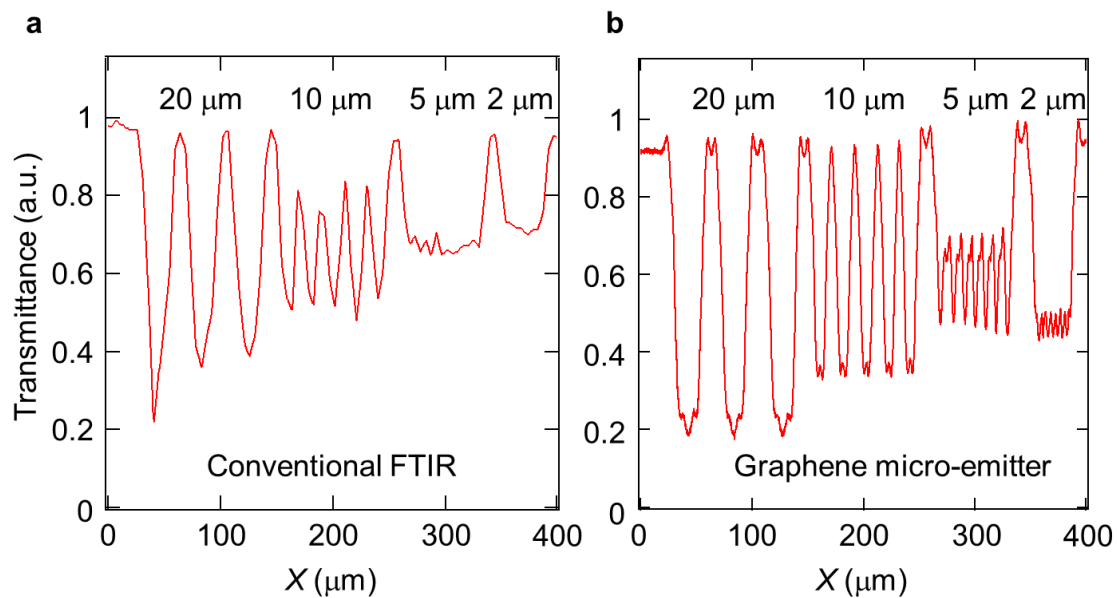
496 corrected by a Cassegrain objective ($\times 40$) placed above the vacuum chamber through the sapphire

497 optical window. For the measurement of the IR imaging, the specimen is mounted to the XYZ piezo

498 motor stage. The specimen is brought into close contact to the graphene micro-emitter, and IR

499 transmittance (absorption) images are obtained by scanning the sample in XY plane

500



501

502 **Extended Data Fig. 3 | Comparison of the spatial dispersion between conventional FTIR and**

503 **graphene micro-emitter. a,b,** Transmittance of one-dimensional line scan along the X axis direction

504 by using conventional FTIR (a) and the unsuspended graphene micro-emitter ($0.5 \times 0.5 \mu\text{m}^2$) (b).

505 Clear periodical modulation of the transmittance can be observed for all line/space pattern by using

506 the graphene micro-emitter in contrast to the conventional FTIR

507